Contrast inversion in neutral-atom microscopy using atomic cluster beams

Geetika Bhardwaj ● and Pranav R. Shirhatti ●*

Tata Institute of Fundamental Research Hyderabad, 36/P Gopanpally, Hyderabad 500046, Telangana, India

This work explores the possibility of using atomic cluster beams as a probe for neutral-atom microscopy (NAM) measurements. Using a beam of Kr clusters with mean size $\sim 10^4$ atoms/cluster we demonstrate that topographical contrast can be obtained, similar to that in the case of monoatomic beams. Further, using atomically thin films of MoS_2 grown on SiO_2/Si substrate we show that NAM imaging using Kr clusters is also possible in domains where topographical contrast is not expected. Surprisingly, these images show an inverted contrast pattern when compared to the case of monoatomic beams. We attempt to understand these observations on the basis of angular distributions resulting from cluster-surface scattering. Finally, we discuss the implications of these results toward achieving a high lateral resolution neutral-atom microscope using atomic cluster beams as probe, with an estimated ultimate achievable lateral resolution up to 20 nm.

I. INTRODUCTION

Using beams of neutral atoms as a probe to image surfaces, also known as neutral atom microscopy (NAM) or scanning helium microscopy (SHeM, in the case of He atoms), is an emerging microscopy technique that holds the promise of probing surfaces in a soft manner [1,2]. Here, similar to charged particle based methods (such as scanning electron microscopy), an atomic beam typically with incident kinetic energy in the range of 10–500 meV is made incident on the sample of interest and the scattered atoms are detected in a position-sensitive manner to generate a contrast map (image) of the surface. One of the major questions in this area of research is to understand contrast generation mechanisms, which is intimately connected to the underlying atom-surface collision dynamics. Another major challenge is to achieve a high lateral resolution. This is largely constrained by the limited ability to manipulate and control a beam of slow-moving neutral atoms.

In the context of microscopy, several schemes to manipulate neutral-atom beams have been put forward in the past. One approach is to focus atomic beams using precisely prepared surfaces having high reflectivity and appropriate shape, acting as mirrors for atomic beams [3–7]. Another approach has been to use the wave nature of atoms and focus atomic beams using zone plate structures [1,8–11]. Despite several promising developments in these areas, focusing of atomic beams well beyond 1 μm spot size remains a scientific and technological challenge.

Arguably, the most successful strategy to date is based on the pinhole design, where a series of apertures are used to collimate the incident atomic beam, consequently reaching a high lateral resolution. This design is relatively easier to build and has been widely adopted by several groups [12–15]. At present, some of the best images in terms of signal-to-noise ratio [14] and resolution (submicrometer) [2] have been achieved using such pinhole designs. An excellent overview of different NAM designs, following its systematic development and current state of the art is provided in a recent review article by Palau *et al.* [16].

Despite the promising developments in pinhole-based NAM, several challenges still remain to be overcome. The highest achievable lateral resolution is dictated largely by the dimensions of the final collimation aperture (pinhole). Using a smaller pinhole to increase the resolution is necessarily accompanied by a loss of signal-to-noise ratio, as the number of incident particles (and the corresponding scattered signal) decreases. Therefore NAM imaging becomes difficult in the region of submicrometer resolution. Additionally, with pinhole sizes less than 1 μm, diffraction of incident atoms from the aperture starts becoming significant. This causes a lateral spread of the beam, thereby limiting the obtainable resolution for a given working distance. A detailed analysis of this situation using numerical simulations has been carried out by Palau *et al.* [17]. By optimizing the positions of collimating apertures, working distance, and accounting for lateral spread of the incident atomic beam caused by diffraction, they estimate that a resolution of 40 nm is achievable under realistic measurement conditions. It should be noted that such performance remains to be experimentally demonstrated.

In this regard, using beams of atomic clusters as a probe offers some interesting possibilities. Firstly, large atomic density of clusters can compensate for the loss of incident intensity, enabling the use of much smaller pinhole sizes. At the same time, heavier mass of individual clusters means negligible diffraction effects, even in the case of small aperture sizes ($\ll 1$ μm). It is worth pointing out that a necessary prerequisite to evaluate the potential of these possibilities is to understand whether the scattering of atomic clusters from surfaces can give rise to contrast maps or not. In the case in which contrast

---

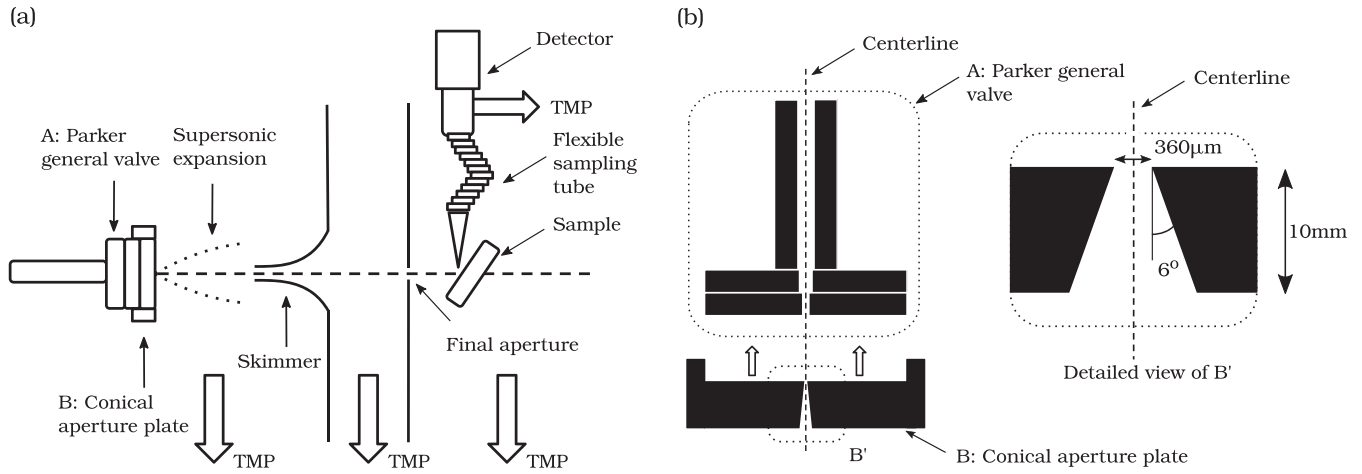*Author to whom correspondence should be addressed: pranavrs@tifrh.res.in

(a)

(b)

FIG. 1. (a) Schematic diagram of the overall experimental setup used for NAM measurements. TMP corresponds to turbomolecular pump. Supersonic expansion from the nozzle is followed by a 200-μm-diameter opening skimmer and a collimation aperture with diameter 50 μm. The collimated beam is made incident from the target sample, placed on a pair of piezo stages (XY), in the scattering chamber. A fraction of the scattered flux around the specular direction (acceptance angle of $\sim$32°) enters via the sampling aperture (1 mm opening diameter) into the sampling tube, connected to a quadrupole mass spectrometer with differential pumping arrangement. (b) Schematic diagram of the pulsed nozzle source and a custom-built conical aperture plate (to aid in cluster formation). A detailed view of the conical aperture plate is shown on the right.

is observed, what is its nature and how does it compare with the usual scenario of monoatomic beams? These questions form the subject of our present study.

In the forthcoming sections, we describe the experimental methods used to produce and characterize atomic cluster beams. Following this, we discuss the results of NAM measurements using Kr clusters in topographical and beyond topographical contrast regimes, where a contrast inversion is seen. We discuss the possible origins of this unusual contrast inversion and implications of these findings toward developing a high-resolution NAM.

II. EXPERIMENTAL SETUP

Experimental setup and sample preparation procedure used in the present work is largely the same as in our previous work [15]. Only specific features essential to understand the present work are described in detail below. Figure 1(a) shows a schematic diagram of the experimental setup used in this work. A pulsed atomic beam source comprising the following components was used: (a) pulsed solenoid valve (Parker 009-1643-900; orifice diameter = 0.5 mm) and (b) a custom-built aperture plate with a 10-mm-long conical opening with the diameter of the smaller orifice being 360 μm and a half opening angle of 6° [Fig. 1(b)]. This aperture plate was mounted on the front plate of the pulsed valve while keeping their centers aligned. He or Kr gas was allowed to expand supersonically from this atomic beam source into the source chamber. A 200-μm skimmer was used to extract the centerline intensity from the gas expansion forming a beam in the first differential chamber. Finally, a 50-μm aperture, placed inline, was used to obtain a collimated beam. The width (full width at half maximum, FWHM) of He and Kr beams, measured at a distance of 15 mm (sample plane) from the final collimation aperture using a knife-edge scanning method, were observed

to be 60 and 56 μm, respectively (see Appendix A). These correspond to an angular divergence of < 1 mrad. For He and Kr beams, based on the pressure changes observed in the detection chamber with the molecular beam on and off (without the sample), we estimate that each gas pulse consists of approximately 10^{10} atoms being incident on the sample. This corresponds to a flux of $\sim$$10^{16}$ atoms/(s sr).

The estimated incident energy of the pure He beam is 65 meV while that for Kr monomers in 50% Kr + 50% He mixture, is 124 meV. For Kr_n clusters produced using the same mixture it is estimated to be approximately $n \times 124$ meV. These estimations are obtained using the well-known relation of terminal velocity in the case of supersonic expansions [18] and are also described in more detail in our previous work [15]. The collimated beam scatters from the sample placed on a movable platform (XY) comprised of two piezoelectric stages stacked over each other, housed in the detection chamber.

A 180-mm-long flexible stainless steel bellow (inner diameter approximately 3.6 mm) was used as a sampling tube with an orifice of diameter 1 mm drilled at its end. One end of the sampling tube was mounted on a single-axis manipulator, enabling measurement of the scattered signal at different angular positions. In this setup the angular distribution measurements were limited to a plane perpendicular to the scattering plane (Fig. 2). A significant distortion was observed in our attempts (results not shown here) in measuring in-plane angular distributions. Hence, we restrict ourselves to report and discuss only the out-of-plane scattered distributions in this work.

For NAM measurements, the pulsed valve was driven by a pulse valve driver (Iota One, 060-0001-900; Parker). Opening time was set to 25 ms and the repetition rate at 2 Hz. Under these conditions, the steady-state pressures in the source, first differential, and detection chamber were 3×10^{-4}, 5×10^{-6}, and 3×10^{-7} mbars, respectively. Quadrupole mass
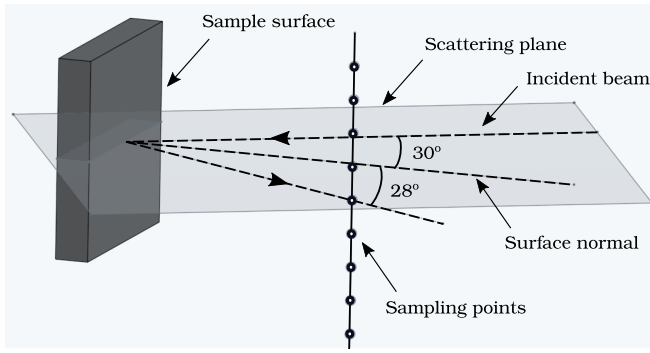
FIG. 2. Schematic representation of the experimental arrangement used for the angular distribution measurements. Sampling points represent the positions where the measurements were made (perpendicular to the scattering plane) using a flexible sampling tube mounted on a single-axis manipulator. At present, this arrangement limits us to measure only out-of-plane angular distributions.

spectrometer (Stanford Research System; Residual Gas Analyzer 200) was used as a detector and its sampling rate was set to 40 Hz. The resulting signal corresponded to pulses of 250–300 ms being detected. Channeltron voltage was set to -1560 V corresponding to a nominal gain of 1.2×10^4. The dwell time at each sample position (pixel) was set to 2.5–3.5 s depending on the signal-to-noise ratio and the overall duration of each measurement.

The additional aperture plate with a long conical orifice was used to aid in the formation of large clusters. The relation among average cluster size produced by a nozzle is described empirically by determining the scaling parameter (Γ^*) as given below [19–23]:

$$\Gamma^* = k \frac{(d / \tan \alpha)^{0.85} P_0}{T_0^{2.29}}.$$

Here, k is the gas-dependent condensation parameter [22–24]—4 for He, 1700 for Ar, 2900 for Kr; α is the half-angle of the conical aperture (in degrees); d is the orifice diameter (in micrometers); P_0 is the backing pressure (in millibars), and T_0 is the initial gas temperature (in kelvin).

In the present experiments a mixture of 50% Kr in He was used for NAM measurements with clusters as it resulted in the highest signal observed (see Appendix B). In this case $\Gamma^* \approx 1.6 \times 10^4$ (at 6 bars backing pressure). Under these conditions, based on the previously reported scaling relations among Γ^*, average cluster size, and condensation fraction [20,24,25], nearly all Kr atoms are expected to be in cluster form with a mean size of 10^4 atoms/cluster. On the other hand, for pure He beams under similar conditions, Γ^* is 17 at 2 bars and 86 at 10 bars. Therefore, He beams are expected to be largely monoatomic in nature with negligible cluster formation. Additional measurements to characterize cluster formation were carried out by means of measuring the change in centerline intensity as a function of backing pressure (see Appendix B) and x-ray generation by intense femtosecond laser ionization (see Appendix C).

Samples of MoS_2 grown on SiO_2/Si substrate used in the present study were prepared using a chemical vapor deposition method and characterized using optical microscopy and

Raman spectroscopy, as described previously [15]. Features on a typical sample consist of bare substrate, thin (one to three layers) and thick (more than six layers). Here one monolayer corresponds to a thickness of 0.65 nm [26]. These features correspond to the purple, blue, and light-blue colors in the optical microscopy images obtained using white light illumination, respectively (see Figs. 4 and 5).

III. RESULTS AND DISCUSSIONS

A. Generation of topographical contrast with Kr clusters

Topographic contrast is the most commonly observed contrast in NAM images [9]. It arises in the regime where incident atoms undergo diffuse scattering upon impact with the surface, and spatial features of interest are much larger than the beam spot size. Under these conditions NAM images closely resemble the geometric features of the sample. As far as clusters are concerned, *a priori* it is not obvious whether simple topographical contrast, commonly seen with monoatomic beams, can be observed or not. This ambiguity stems from the fact that the extent of thermalization of Kr atoms, in the form of large clusters, upon impact with the surface is unknown.

In order to understand whether topographic contrast is generated or not, we first image a microscopically rough object (a fine-pitched stainless-steel screw; pitch $= 300$ μm) using both monoatomic helium and krypton cluster beams. Features being imaged in this case are much larger than the incident beam size and we can expect to see images largely governed by topographical contrast. Figure 3(a) shows an optical image of the screw. Panels (b) and (c) show NAM images of a small portion of the screw [marked by a white rectangle in panel (a)], obtained using a beam of helium and krypton clusters, respectively. Panel (d) shows an optical image depicting the side view of the screw edge. Panels (e) and (f) depict the line profiles corresponding to the optical image shown in (d), measured using He atoms and Kr clusters, respectively. Quite clearly, the NAM images obtained using a beam of He (monoatomic) and Kr (clusters) show a one-to-one correspondence with the optical images. We conclude that large atomic cluster beams are well capable of generating topographical contrast. We also infer that Kr atoms get thermalized on the surface to a large extent.

These results are of potential interest toward developing a high-resolution NAM. In measurements with monoatomic beams such as He, diffraction of incident atoms from the final aperture sets the ultimate limit to the highest achievable lateral resolution. For He atoms, using numerical modeling, this limit has been estimated to be approximately 40 nm [17]. Large atomic clusters such as those used in our experiments, owing to their much higher mass ($\gg 10^4$ times compared to helium atoms), are expected to behave like classical particles. Consequently, the diffraction effects will be negligible even for very small pinhole sizes, providing a route to achieve higher lateral resolutions compared to monoatomic beams. In addition, the higher density offered by atomic clusters can lead to much higher incident and scattered signals even with smaller aperture sizes. We believe that the ultimate limit in this case is likely to be
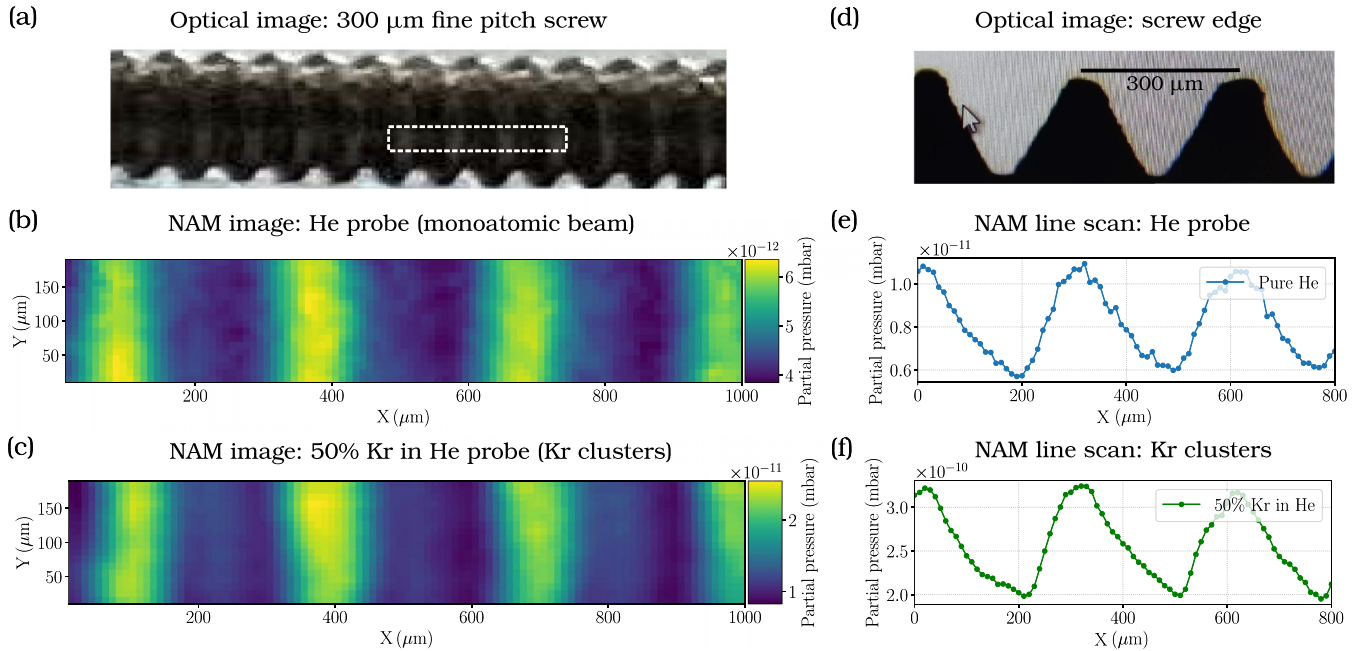
FIG. 3. (a) Optical image of a 300-μm fine-pitch screw (outer diameter of 1.5 mm). A small region marked by a white dashed rectangle was selected to perform the NAM measurements. (b) and (c) NAM image using a monoatomic beam of He atoms with a backing pressure of 1.5 bars and Kr clusters (step size of 20 μm) with a backing pressure of 6 bars, respectively. (d) Optical image of the edge of screw. (e) and (f) Line scan performed along the screw length using a beam of monoatomic He (1.5 bars of backing pressure) and Kr clusters (6 bars of backing pressure), respectively (step size 10 μm). All the NAM measurements were performed using the custom-built nozzle shown in Fig. 1(b) with pulse duration set to 25 ms, at a repetition rate of 2 Hz. The intensity scale in NAM images refers to partial pressure corresponding to the scattered flux in millibar units.

set by the interaction of incident atomic clusters with the edge of the small pinhole they are sent through. At distances where interatomic binding energy of the cluster becomes comparable to the interaction energy with atoms constituting the edge of the pinhole, one can expect the clusters to fragment as they travel across the aperture. Given that these interactions are of van der Waals type, such forces will be significant only at nanometer length scales. In principle, this can allow the use of small pinholes for collimation, with sizes approaching that of the cluster itself. As an example, in the present case of Kr cluster beams the mean cluster size is estimated to be 10^4 Kr atoms. Assuming that the clusters larger than 10^5 Kr atoms constitute a negligibly small fraction, we estimate the minimum pinhole size needed for the incident clusters to travel undisturbed. For a Kr cluster of 10^5 atoms, assuming spherical shape and a density of 3.2 g/cm^3, the diameter is about 20 nm. It is reasonable to think that this presents the ultimate limit to the final collimation pinhole size and consequently the highest achievable lateral resolution under these measurement conditions.

B. Beyond topographical contrast: Inverted contrast with Kr clusters

Regimes beyond topographic contrast correspond to situations where specific details of atom-surface collision play an important role in contrast generation. This is unlike the case of topographic contrast resulting from diffuse scattering, where there is no correlation among the incident and the final

momentum of scattered particles. As an example, chemical contrast [28] has been hypothesized to arise from surface specific inelastic scattering with phonons, leading to a contrast dependent on the surface chemical composition. Contrast arising due to diffraction of the incident atomic beam as a result of scattering from surfaces with local crystalline order has also been reported recently [29]. In our previous work, it was shown that using atom scattering based microscopy, thin films up to a single monolayer of MoS_2 on SiO_2/Si can be successfully imaged using a 20–30-μm-sized beam of He and/or Kr atoms as an incident probe. Further it was also observed that the contrast decreased with lowering incident energy [15]. These results point toward the fact that contrast mechanisms beyond simple topographical in nature are at play. Here, we investigate whether NAM imaging of atomically thin layers of MoS_2, in the beyond topographic contrast regime, is possible with a beam of Kr clusters or not.

Measurements with a monoatomic beam of He and Kr atoms, produced with a 20-μm continuous nozzle, can be seen in Fig. 4. Panel (a) shows an optical image of a small portion of MoS_2 grown on SiO_2/Si substrate and the corresponding NAM images obtained with He and Kr beams are depicted in (b) and (c), respectively. The scattered flux of He and Kr from MoS_2 is consistently higher as compared to SiO_2/Si in both cases and a clear one-to-one correspondence is seen. Such kind of contrast generation with the underlying possible reasons have been discussed in our previous work [15].

Measurements performed with a beam of Kr clusters and a monoatomic beam of He are shown in Fig. 5. Panels 5(a)–5(e) show optical images of small portions of independently
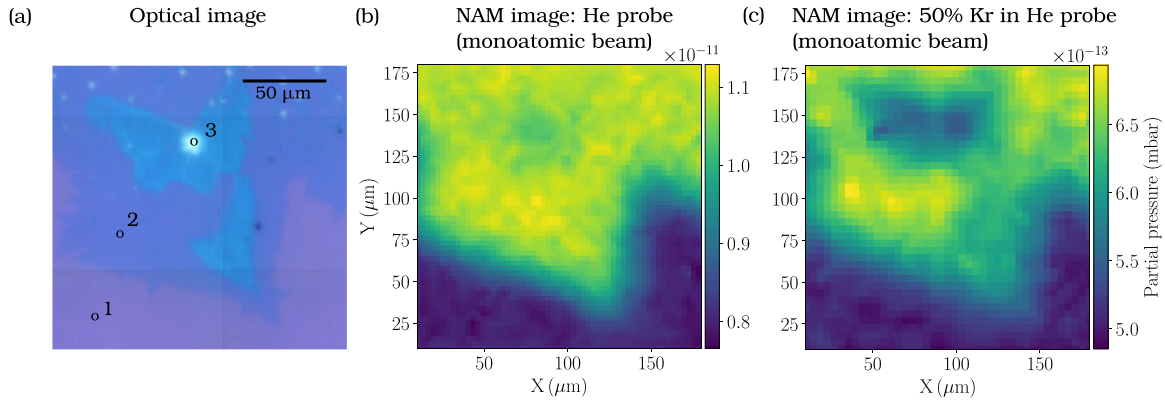
FIG. 4. (a) Optical image of a small portion of the MoS_2 sample where purple, blue, and light-blue colored regions, marked by 1, 2 and 3, correspond to SiO_2/Si substrate, thin and thick layers of MoS_2 [15,27]. (b) and (c) NAM images obtained using a continuous nozzle with 20-μm orifice diameter with a monoatomic beam of He and Kr atoms as probe, respectively (with a backing pressure of 6 bars in both the images). The scattered flux from MoS_2 is consistently higher than SiO_2/Si substrate in both cases. The intensity scale in NAM images refers to partial pressure corresponding to the scattered flux in millibar units.

prepared samples of MoS_2 films on SiO_2/Si substrate. NAM measurements using He atom beam are shown in Figs. 5(f) and 5(j). Here we observe the expected contrast pattern as seen previously with monoatomic beams (Fig. 4), i.e., higher scattered flux from the MoS_2 surface as compared to SiO_2/Si. Figures 5(g)–5(i) show the images obtained using Kr clusters. Again, a one-to-one correspondence with the optical images is seen, but interestingly, contrast patterns appear inverted. Here, a larger signal for scattered Kr is obtained from SiO_2/Si substrate as compared to regions covered with MoS_2. It is worth pointing out that NAM measurements using He atoms (monomers) performed before and after the measurements done with Kr clusters (on the same region) do not show any significant changes. Based on this we conclude that collision-induced damage caused by the impact of large Kr clusters (even with incident kinetic energy of the order of 10^3 eV) is negligible under our measurement conditions (see Appendix D). Interestingly, scattering of large Kr clusters does not simply lead to diffuse scattering alone and seems to be sensitive to the surface characteristics. Observation of such a contrast inversion merits further discussion.

Previous studies on scattering of atomic and molecular clusters from surfaces offer valuable insights in this direction. Gspann and Krieg [30] have studied scattering of clusters of He ($\langle n \rangle = 105$), H_2 ($\langle n \rangle = 10^4$), and N_2 ($\langle n \rangle = 10^4$) from polished stainless-steel surfaces ($\langle n \rangle$ corresponds to the average cluster size). At incident angles of $84.3°$ from surface normal, angular distribution measurements for scattered H_2 and N_2 clusters were observed to peak at supraspecular angles (beyond specular direction, away from surface normal). Holland *et al.* [31] have studied scattering of large N_2 clusters ($n = 10^4$) from atomically flat, clean, single-crystal surfaces of Fe(110), Fe(111), and Ag(111), prepared under UHV conditions. They report that irrespective of the surface chosen in their measurements, angular distributions of the scattered particles peak in the supraspecular direction, especially for large incident angles from surface normal. They also note that upon using a rough surface as a target (prepared by ion bombardment without annealing), the supraspecular scattered

peak becomes less pronounced and the angular distributions tend toward diffuse scattering. Similar observations have been reported for scattering of Ar clusters [32] and N_2 clusters ($n = 200$–1000) from graphite surface [33].

Xu *et al.* [34] have studied the scattering of small Ar clusters ($n = 5$–26) using classical stochastic trajectory simulations. Although the cluster sizes studied here are relatively small, the simulations show similar trends as observed in the above-mentioned experiments. Svanberg *et al.* [35] have extended the above work by performing simulations for relatively large Ar clusters ($n = 100$–4400) with incidence energy of 63 meV/atom, scattering from the Pt(111) surface. Their simulations also show that the angular distributions peak in the supraspecular direction. In summary, previous studies based on both experiments and simulations, show that for larger clusters the scattered angular distributions peak in the supraspecular direction. Additionally, on rough surfaces this pronounced supraspecular scattering becomes weaker and tends more toward diffuse scattering.

This general aspect of cluster scattering from surfaces seems significant as far as our observation of contrast inversion is concerned. For monoatomic beams, the scattered flux is expected to peak close to the specular direction in the case of elastic scattering or toward the surface normal, in the case of a large diffuse scattering component. On the other hand, for large Kr clusters ($\langle n \rangle \sim 10^4$), the majority of the scattered flux is likely to exit at large angles from surface normal, in the supraspecular direction. Given that our sampling aperture is placed near the specular direction, a large fraction of the supraspecular scattered atoms will not be captured by the detector. Our previous study has shown that at an atomic scale, MoS_2 surfaces are generally smoother than the SiO_2/Si substrate [15]. Given the above points, we hypothesize that on the MoS_2 surface, supraspecular scattering leads to relatively fewer atoms entering the collection aperture placed along the specular direction. At the same time, the increased roughness on SiO_2/Si substrate can lead to more diffuse scattering-like behavior, resulting in a relatively higher scattered signal being detected.
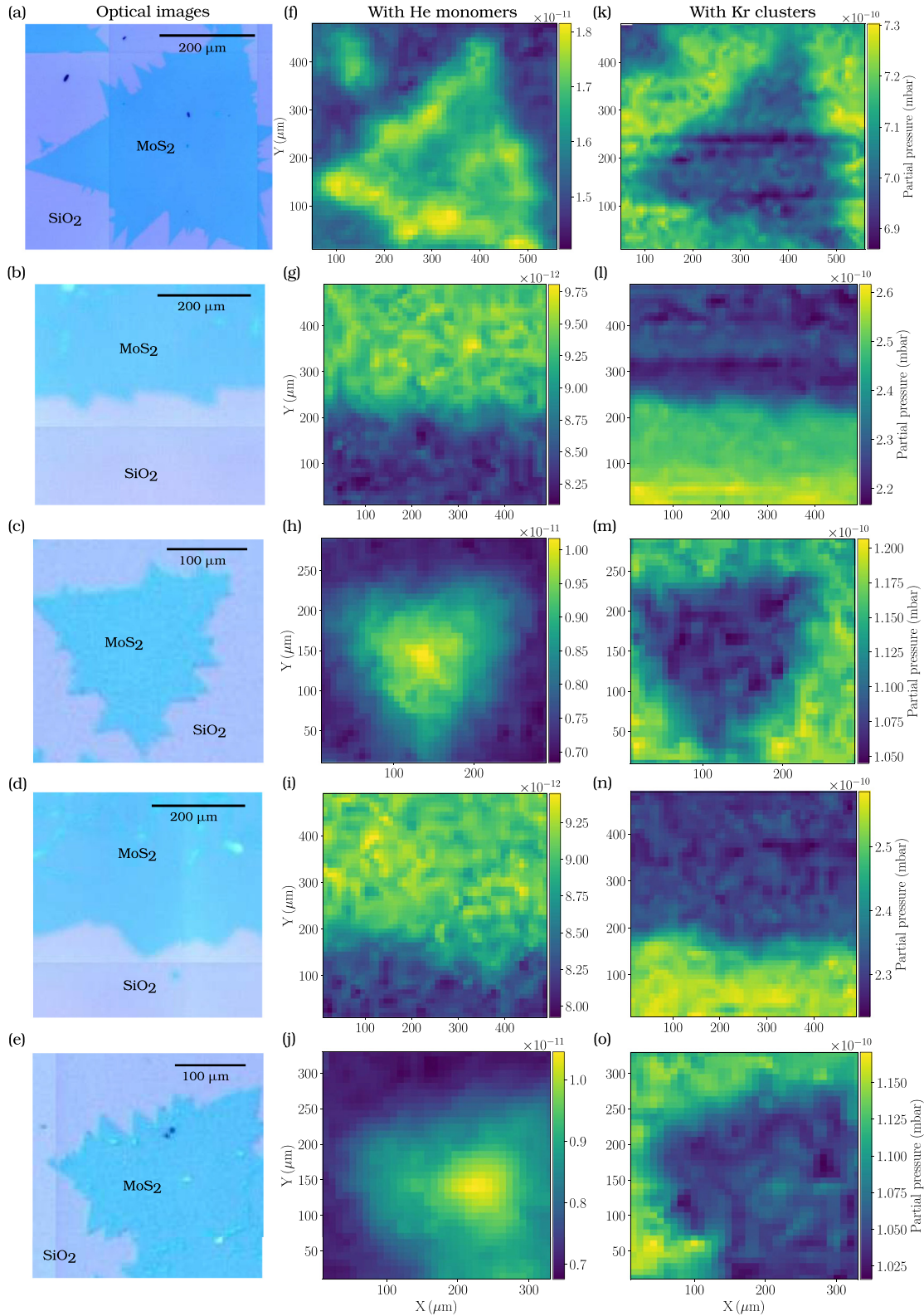
FIG. 5. (a)–(e) Optical images of five small portions of independently prepared MoS_2 films on SiO_2/Si samples. In all the samples, MoS_2 and SiO_2 regions have been marked. Blue regions contain thin layers, one to three monolayers of MoS_2. (f)–(j) NAM images of the same samples using beams of monoatomic He atoms with a backing pressure of 1.5 bars. (k)–(o) NAM images of the same samples using beams of Kr clusters (mean size of 10^4 atoms; see text) with a backing pressure of 6 bars. NAM images with both He and Kr clusters show one-to-one correspondence with the optical images. Interestingly, images obtained with Kr clusters show an inverted contrast to that compared with He. For all NAM measurements shown here, the pulse duration was set to 25 ms and the repetition rate to 2 Hz. The intensity scale in the NAM images refers to partial pressure corresponding to the scattered flux in millibar units.
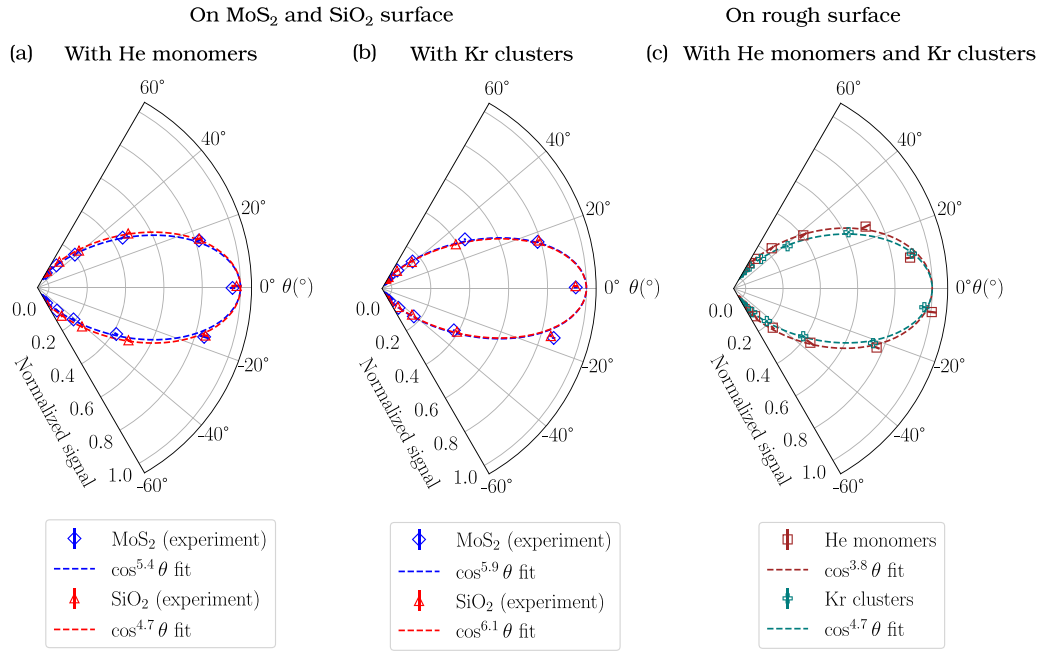
FIG. 6. (a) and (b) Angle-resolved scattered flux (perpendicular to scattering plane) from MoS_2 and SiO_2/Si substrate using a beam of monoatomic He atoms and Kr clusters. For He, the distribution obtained from the MoS_2 surface is slightly narrower than that of the SiO_2 surface, consistent with the observed contrast pattern. In the case of Kr clusters, both the distributions (b) look very similar. Angular distribution obtained from a rough stainless-steel surface is shown in (c) for comparison. The angular position of $0°$ corresponds to the surface normal.

Besides the above possibility, other systematic differences could also be at play here. MoS_2 films are bound to the lower layers or SiO_2/Si substrate by relatively weak van der Waals interaction. As a result, MoS_2 surface acts as a relatively softer landing site for Kr clusters. Large Kr clusters having sizable incidence energy compared to its monoatomic counterparts, when scattered from a relatively softer surface (compared to SiO_2/Si) can lead to a broad scattered distribution. Consequently, a lower flux will be measured by the detector placed in the specular direction compared to scattering from a relatively rigid SiO_2/Si surface, consistent with the inverted contrast observed in our measurements. The effect of rigidity of thin films on the scattered angular distributions have been studied by Taleb *et al.* [36] by studying the heavy vs light atom scattering from graphene surface in the case of weak and strong interactions with the substrate. They observed that in the case of weak interaction with substrate [Gr/Ir(111)], neon atoms scattered largely inelastically leading to a broad angular distribution. On the other hand, scattering from a more strongly bound substrate such as Gr/Ni(111), sharp diffraction peaks were obtained.

In order to understand these points better, we resort to angle-resolved measurements. Figures 6(a) and 6(b) show a comparison of the angular distributions resulting from scattering on SiO_2/Si and MoS_2 surfaces, obtained using He (monoatomic) and Kr (clusters), respectively. Angular distributions from a microscopically rough surface (stainless-steel screw, shown in Fig. 3) are also shown in (c) for the sake of comparison. It should be noted that these distributions were measured for an out-of-plane scattering configuration (see Fig. 2) and are not corrected for any distortions resulting

from the measurement configuration. Nonetheless, a systematic comparison of the relative changes based on these results is still possible.

A common feature observed in the case of MoS_2 and SiO_2/Si is that angular distributions obtained using monoatomic He are rather broad and only slightly narrower than that observed from a rough surface. This indicates that a substantial fraction of the atoms undergo diffuse scattering. This is expected since our samples were placed in a vacuum chamber operating at a base pressure of 3×10^{-7} mbars and not true ultrahigh vacuum conditions. Further, no *in situ* sample cleaning was done. Under these conditions, a significant amount of adsorbates will be present on the surface, leading to a large diffuse scattering component. For the He beam, the width of the distribution in the case of the MoS_2 surface, is somewhat narrower than SiO_2/Si substrate, consistent with the contrast observed in NAM images. Angular distributions obtained with Kr clusters appear very similar for MoS_2 and SiO_2/Si. Given that these distributions almost look the same and the fact that we see an inverted contrast pattern, we infer that the changes are largely occurring in the in-plane scattering distributions. This is also expected from previous studies showing supraspecular scattering. A clear answer to these questions can be obtained by in-plane angle-resolved measurements, which are currently unavailable in our setup. An upgraded version with provision for measuring both in-plane and out-of-plane angular distributions with the aid of a combined rotation and linear manipulator along with sample heating capability (for removing weakly bound adsorbates) is being designed in our laboratory for future studies.
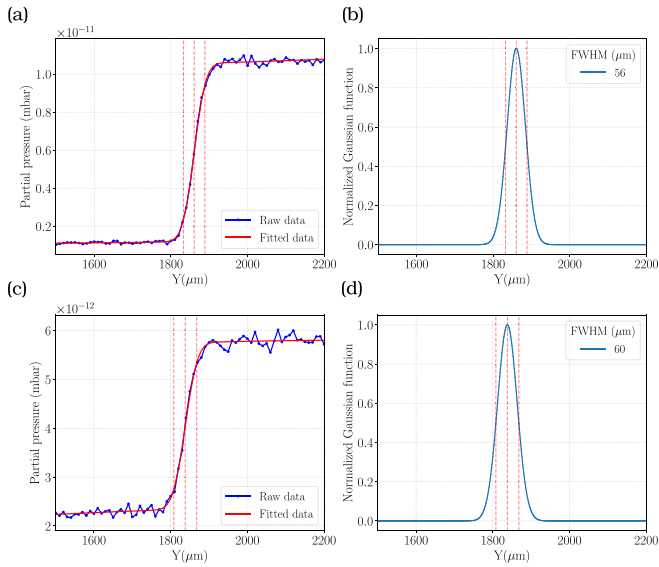
FIG. 7. Incident beam-width estimation on the sample plane using a knife-edge scanning method. (a) Beam-width measurement for Kr in 50% Kr + 50% He mixture. Blue curve shows the signal of Kr observed as a function of the position of the knife edge (razor blade) with a step size of 10 μm. Red curve shows the best fit, using a model based on a step function convoluted with a Gaussian. (b) Modeled beam profile with the parameters obtained by fitting with a FWHM of 56 μm. (c) and (d) depict the same for pure He (monoatomic) resulting in a beam-width estimate of 60 μm (FWHM).

IV. CONCLUDING REMARKS

In this work we have demonstrated that NAM imaging is possible using a beam of Kr atom clusters and the well-known topographic contrast can be obtained for rough surfaces. Using samples of atomically thin films of MoS_2 grown on SiO_2/Si substrate, we have shown that NAM imaging with Kr clusters is possible even in the regime of beyond simple topographical contrast. Interestingly, here we observe a contrast inversion compared to the similar measurements made with monoatomic beams.

Importantly, the results presented here clearly establish that NAM imaging can be done with atomic clusters as well. To the best of our knowledge, this possibility has not been explored previously. These results point toward two interesting possibilities in the direction of developing a high lateral resolution NAM. Firstly, the higher atomic density of clusters can be exploited to obtain high incident beam flux that can in turn allow the use of smaller pinholes leading to higher lateral resolution. Secondly, in the case of atomic clusters, owing to their much higher mass compared to their monoatomic counterparts, the problem of lateral spread caused by diffraction from small pinholes is expected to be negligible. Based on the sizes of the incident clusters, we estimate that small pinholes up to 20 nm can be used, opening a possible route toward realizing a high lateral resolution neutral-atom microscope.

A systematic exploration of these possibilities will be needed, especially to understand the maximum centerline intensity obtainable in the case of atomic cluster beams [37]. Here, the role of mass focusing effect [38] toward enhancing the density of clusters along the centerline and the counteracting effect of warming up of the beam to reduce the centerline intensity need to be understood well. Further, these results also suggest an interesting possibility of developing a guided negatively charged cluster-ion source with subsequent neutralization. Using this approach, a tightly focused beam of low-energy neutral atomic clusters can be generated. Such focused neutral atomic cluster beam sources can also be of interest for developing a high lateral resolution NAM.
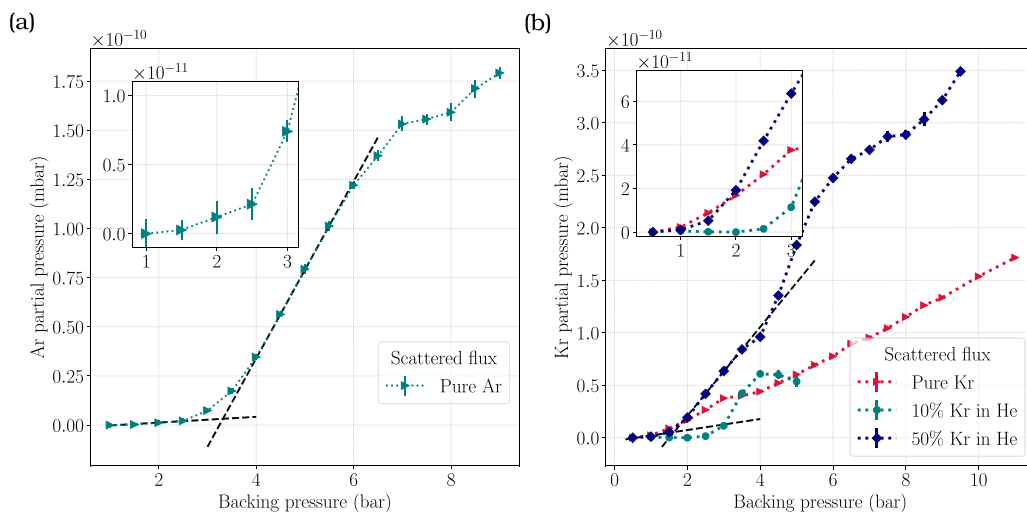
FIG. 8. Ar (a) and Kr (b) signal along centerline with increasing backing pressure. These measurements were made by monitoring the scattered signal from a rough surface. The solid lines show the linear fits in different pressure ranges.
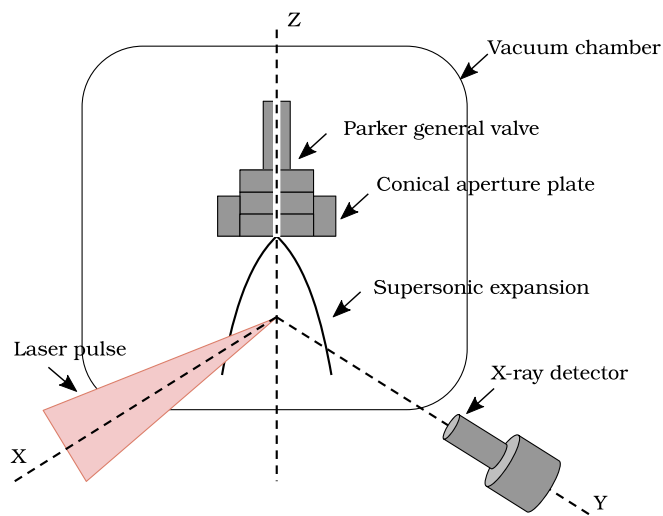
FIG. 9. Schematic diagram of the experimental setup used to study the femtosecond laser ionization and consequent x-ray generation from the beams of Ar and Kr clusters.

APPENDIX A: INCIDENT BEAM-WIDTH ESTIMATION

Beam-width estimation of a monoatomic He beam and a beam of Kr clusters (using a 50% mixture) were measured using a knife-edge scanning method. These results are shown in Fig. 7.
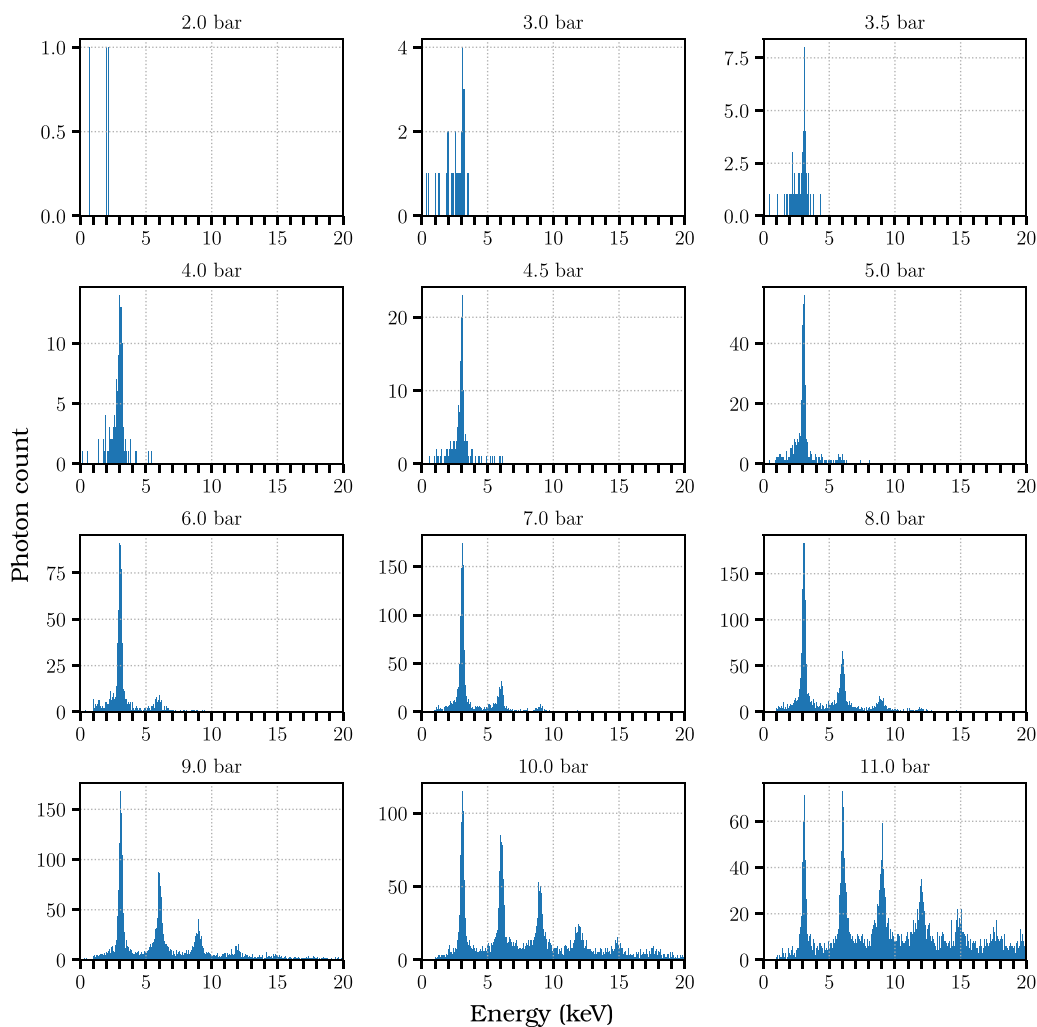

FIG. 10. Spectrum of the x rays generated from Ar clusters interacting with intense femtosecond laser pulses, measured at different backing pressures. Actual transition is at an energy of 3 keV. Peaks at 6, 9, 12, 15, and 18 keV energies merely indicate the accumulation of 2, 3, 4, 5, and 6 x-ray photons within the dead time of detector, respectively.
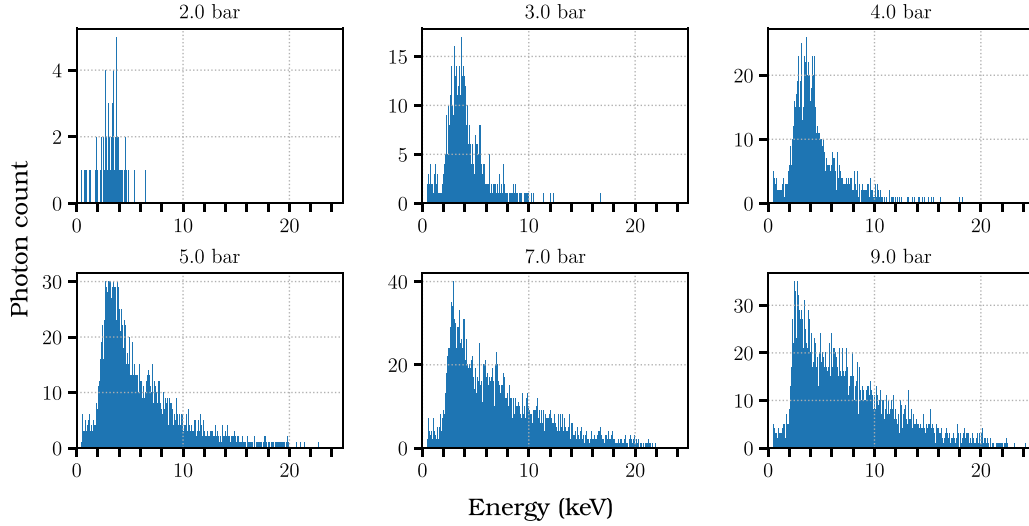
FIG. 11. Spectrum of the x rays generated from Kr clusters interacting with intense femtosecond laser pulses, measured at different backing pressures (pure Kr). Here we do not observe the separated peaks as in the case of Ar. Rather, a continuum (inverse bremsstrahlung) was observed, as expected for larger atoms.

APPENDIX B: VARIATION IN SCATTERED SIGNAL WITH BACKING PRESSURE

Centerline intensity of a molecular beam is related to the backing pressure by the following relation:

$$I_0 \propto \frac{P_0 d^2}{\sqrt{T_0}}. \tag{B1}$$

Here, d is the orifice diameter, and P_0 and T_0 are the backing pressure and temperature, respectively. According to the above relation, Kr signal is expected to increase linearly with increasing backing pressure. However, we see a change in the slope for Ar at 3 bars and Kr beams in the range of 1–2.5 bars (Fig. 8). We infer this change in slope to be caused by the onset of formation of large clusters, as suggested by the Hagena parameter. Further evidence for large cluster formation was obtained by performing femtosecond laser ionization, leading to characteristic x-ray emission being observed for Ar and Kr.

APPENDIX C: EXPERIMENTAL SETUP TO VERIFY CLUSTER FORMATION USING X-RAY GENERATION

Experimental setup used for x-ray generation and detection from Ar and Kr clusters is depicted in Fig. 9. These measurements were performed with the same pulsed nozzle (with similar operating parameters) as used for NAM. Focused pulses with a temporal width 25 fs (at 800 nm) having an energy of 2 mJ/pulse (intensity $\sim$$10^{16}$ W/cm^2) were made incident at the center of supersonic expansion, approximately 5 mm away from the exit plane. This interaction generated x rays that were detected using a Si-PIN detector (Amptek XR-100CR). A significant amount of x-ray emission was observed under these conditions, clearly indicating that large clusters with sizes of the order of 10^4 atoms were formed for both Ar and Kr (Figs. 10 and 11).
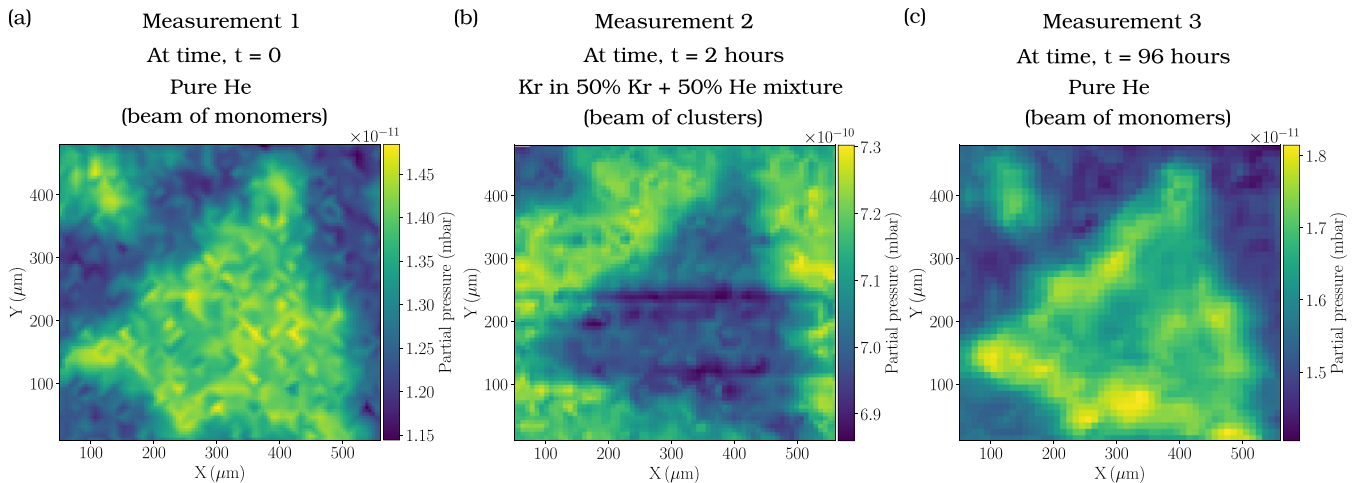

FIG. 12. (a) NAM image measured with pure He with a backing pressure of 1.5 bars at time $t = 0$. (b) Measurement performed with Kr in 50% Kr and He mixture with a backing pressure of 6 bars at time $t = 2$ h. (c) Measurement performed with pure He with a backing pressure of 1.5 bars at time $t = 96$ h.

APPENDIX D: SEQUENTIAL MEASUREMENT WITH PURE HELIUM, 50% KRYPTON, AND PURE HELIUM

Figure 12 shows the results of NAM measurements with He monomers (a), followed by measurement with Kr clusters (b) and again with He monomers (c). Images (a) and (c) show a similar contrast pattern and based on this we conclude that the Kr clusters do not cause any significant change on the sample surface under our measurement conditions.

[1] D. A. MacLaren, B. Holst, D. J. Riley, and W. Allison, Focusing elements and design considerations for a scanning helium microscope (SHeM), Surf. Rev. Lett. **10**, 249 (2003).

[2] P. Witham and E. Sánchez, Exploring neutral atom microscopy: Exploring neutral atom microscopy, Cryst. Res. Technol. **49**, 690 (2014).

[3] B. Holst and W. Allison, An atom-focusing mirror, Nature (London) **390**, 244 (1997).

[4] K. Fladischer, H. Reingruber, T. Reisinger, V. Mayrhofer, W. E. Ernst, A. E. Ross, D. A. MacLaren, W. Allison, D. Litwin, J. Galas *et al.*, An ellipsoidal mirror for focusing neutral atomic and molecular beams, New J. Phys. **12**, 033018 (2010).

[5] G. Anemone, A. A. Taleb, S. D. Eder, B. Holst, and D. Farías, Flexible thin metal crystals as focusing mirrors for neutral atomic beams, Phys. Rev. B **95**, 205428 (2017).

[6] P. Sutter, M. Minniti, P. Albrecht, D. Farías, R. Miranda, and E. Sutter, A high-reflectivity, ambient-stable graphene mirror for neutral atomic and molecular beams, Appl. Phys. Lett. **99**, 211907 (2011).

[7] D. Barredo, F. Calleja, P. Nieto, J. J. Hinarejos, G. Laurent, A. L. Vázquez de Parga, D. Farías, and R. Miranda, A quantum-stabilized mirror for atoms, Adv. Mater. **20**, 3492 (2008).

[8] R. B. Doak, R. E. Grisenti, S. Rehbein, G. Schmahl, J. P. Toennies, and C. Wöll, Towards Realization of an Atomic de Broglie Microscope: Helium Atom Focusing Using Fresnel Zone Plates, Phys. Rev. Lett. **83**, 4229 (1999).

[9] M. Koch, S. Rehbein, G. Schmahl, T. Reisinger, G. Bracco, W. E. Ernst, and B. Holst, Imaging with neutral atoms—a new matter-wave microscope, J. Microsc. **229**, 1 (2008).

[10] T. Reisinger and B. Holst, Neutral atom and molecule focusing using a Fresnel zone plate, J. Vac. Sci. Technol. B **26**, 2374 (2008).

[11] A. S. Palau, G. Bracco, and B. Holst, Theoretical model of the helium zone plate microscope, Phys. Rev. A **95**, 013611 (2017).

[12] P. Witham and E. Sánchez, A simple approach to neutral atom microscopy, Rev. Sci. Instrum. **82**, 103705 (2011).

[13] M. Barr, A. Fahy, A. Jardine, J. Ellis, D. Ward, D. A. MacLaren, W. Allison, and P. C. Dastoor, A design for a pinhole scanning helium microscope, Nucl. Instrum. Methods Phys. Res. Sect. B **340**, 76 (2014).

[14] A. Fahy, M. Barr, J. Martens, and P. C. Dastoor, A highly contrasting scanning helium microscope, Rev. Sci. Instrum. **86**, 023704 (2015).

[15] G. Bhardwaj, K. R. Sahoo, R. Sharma, P. Nath, and P. R. Shirhatti, Neutral-atom-scattering-based mapping of atomically thin layers, Phys. Rev. A **105**, 022828 (2022).

[16] A. S. Palau, S. D. Eder, G. Bracco, and B. Holst, Neutral helium microscopy, Ultramicroscopy **251**, 113753 (2023).

[17] A. S. Palau, G. Bracco, and B. Holst, Theoretical model of the helium pinhole microscope, Phys. Rev. A **94**, 063624 (2016).

[18] G. Scoles, *Atomic and Molecular Beam Methods* (Oxford University Press, New York, 1988).

[19] O. F. Hagena and W. Obert, Cluster formation in expanding supersonic jets: Effect of pressure, temperature, nozzle size, and test gas, J. Chem. Phys. **56**, 1793 (1972).

[20] O. F. Hagena, Condensation in free jets: Comparison of rare gases and metals, Z. Phys. D: At. Mol. Clusters **4**, 291 (1987).

[21] O. F. Hagena, Cluster ion sources, Rev. Sci. Instrum. **63**, 2374 (1992).

[22] T. Ditmire, T. Donnelly, A. M. Rubenchik, R. W. Falcone, and M. D. Perry, Interaction of intense laser pulses with atomic clusters, Phys. Rev. A **53**, 3379 (1996).

[23] T. Ditmire, E. Springate, J. W. G. Tisch, Y. L. Shao, M. B. Mason, N. Hay, J. P. Marangos, and M. H. R. Hutchinson, Explosion of atomic clusters heated by high-intensity femtosecond laser pulses, Phys. Rev. A **57**, 369 (1998).

[24] J. Wörmer, V. Guzielski, J. Stapelfeldt, and T. Möller, Fluorescence excitation spectroscopy of xenon clusters in the VUV, Chem. Phys. Lett. **159**, 321 (1989).

[25] F. Dorchies, F. Blasco, T. Caillaud, J. Stevefelt, C. Stenz, A. S. Boldarev, and V. A. Gasilov, Spatial distribution of cluster size and density in supersonic jets as targets for intense laser pulses, Phys. Rev. A **68**, 023201 (2003).

[26] C. Lee, H. Yan, L. E. Brus, T. F Heinz, J. Hone, and S. Ryu, Anomalous lattice vibrations of single-and few-layer MoS_2, ACS Nano **4**, 2695 (2010).

[27] R. F. Frindt, Single crystals of MoS_2 several molecular layers thick, J. Appl. Phys. **37**, 1928 (1966).

[28] M. Barr, A. Fahy, J. Martens, A. P. Jardine, D. J. Ward, J. Ellis, W. Allison, and P. C. Dastoor, Unlocking new contrast in a scanning helium microscope, Nat. Commun. **7**, 10189 (2016).

[29] M. Bergin, S. M. Lambrick, H. Sleath, D. J. Ward, J. Ellis, and A. P. Jardine, Observation of diffraction contrast in scanning helium microscopy, Sci. Rep. **10**, 2053 (2020).

[30] J. Gspann and G. Krieg, Reflection of clusters of helium, hydrogen, and nitrogen as function of the reflector temperature, J. Chem. Phys. **61**, 4037 (1974).

[31] R. J. Holland, G. Q. Xu, J. Levkoff, A. Robertson, and S. L. Bernasek, Experimental studies of the dynamics of nitrogen van der Waals cluster scattering from metal surfaces, J. Chem. Phys. **88**, 7952 (1988).

[32] M. Châtelet, A. De Martino, J. Pettersson, F. Pradère, and H. Vach, Argon cluster scattering from a graphite surface, Chem. Phys. Lett. **196**, 563 (1992).

[33] A. De Martino, M. Châtelet, F. Pradère, E. Fort, and H. Vach, Experimental investigation of large nitrogen cluster scattering from graphite: Translational and rotational distributions of evaporated N_2 molecules, J. Chem. Phys. **111**, 7038 (1999).

[34] G.-Q. Xu, R. J. Holland, S. L. Bernasek, and J. C. Tully, Dynamics of cluster scattering from surfaces, J. Chem. Phys. **90**, 3831 (1989).

[35] M. Svanberg, N. Marković, and J. B. C. Pettersson, Scattering of large argon clusters from a Pt(111) surface with low collision velocities, Chem. Phys. **220**, 137 (1997).

[36] A. A. Taleb, G. Anemone, R. Miranda, and D. Farías, Characterization of interlayer forces in 2D heterostructures using neutral atom scattering, 2D Mater. **5**, 045002 (2018).

[37] N. G. Korobeishchikov, M. A. Roenko, and G. I. Tarantsev, Mean gas cluster size determination from cluster beam cross-section, J. Cluster Sci. **28**, 2529 (2017).

[38] P. K. Sharma, E. L. Knuth, and W. S. Young, Species enrichment due to Mach-number focusing in a molecular-beam mass-spectrometer sampling system, J. Chem. Phys. **64**, 4345 (1976).